3626 *Macromolecules* **2001,** *34,* 3626−3633

Crystallinity and Mechanical Behavior Evolution in Ethylene−Propylene Random Copolymers

Kathryn J. Wright and Alan J. Lesser*

Polymer Science & Engineering Department, University of Massachusetts, Amherst, Massachusetts 01003

Received November 17, 2000; Revised Manuscript Received March 8, 2001

ABSTRACT: This study investigates crystal changes in Ziegler/Natta-based ethylene−propylene random copolymers subjected to room-temperature annealing. These copolymers, which are being considered as a new class of thermoplastic elastomers, exhibit slow crystallization kinetics. This slow crystallization causes subsequent changes in mechanical behavior that take place over days and even weeks. An initial study consisting of four copolymer compositions is conducted. Crystallization is monitored via differential scanning calorimetry (DSC) and wide-angle X-ray diffraction (WAXD) as a function of sample age and composition. For these copolymers WAXD reveals a change in crystal structure from orthorhombic to hexagonal well below the triple point of polyethylene at room temperature and pressure. Mechanical behavior is also monitored in a similar fashion. Evolution of modulus, yield stress, yield strain, and rupture energy are correlated with changes in crystal structure observed through DSC and WAXD.

Introduction

Ethylene−propylene random copolymers with various molecular architectures are emerging as a new class of thermoplastic elastomers. High molecular weight copolymers behave as elastomeric materials because their maximum crystallinity is very low (less than 15%), and they are well above their glass transition temperature (−55 °C). Since these copolymers have highly branched structures and high comonomer content, crystallization is inhibited. This results in the formation of small crystals on the order of nanometers in thickness. These crystals not only serve to reinforce the copolymer but also serve as physical cross-links contributing to its elastomeric nature.

The composition and architecture affect not only the ultimate crystallinity but also the rate at which this crystallinity is achieved. These materials are relatively new, and in-depth crystallization studies of ethylene−α-olefin copolymers have only recently begun.[1−10] Ziegler−Natta-based copolymers with high comonomer content exhibit bimodal crystallization kinetics.[1,2] This is attributed to the resulting branched architecture of the copolymers.

Two crystallization exotherms are commonly observed. The first occurs at a high temperature (HT) with a relatively large exotherm, and the second is depressed to a much lower temperature (LT) with a smaller exotherm. The HT exotherm is attributed to the crystallization of high molecular weight chains with low branching content while the LT exotherm is due to the crystallization of low molecular weight chains with high branching content.[1,2] For this class of copolymers, molecular segregation occurs so readily that these crystallization kinetics can be observed under nonisothermal conditions. The HT crystals are similar to those found in linear low-density polyethylene. Wide-angle X-ray diffraction (WAXD) experiments show that the introduction of short branches into polyethylene via propylene incorporation results in unit cell dimensions slightly enlarged to accommodate the additional methyl groups.[11]

Table 1. Ethylene−Propylene Copolymer Compositions

sample	% ethylene	M_w	M_w/M_n	no. of SCB/1000C	comonomer distribution
A	58.1	153 000	2.1	210	homogeneous
B	68.6	108 000	1.4	158	heterogeneous
C	69.0	149 000	1.5	154	heterogeneous
D	79.8	111 000	1.9	99	homogneous

The structure of polyethylene (PE) is well-characterized. On a pressure−temperature phase diagram for PE, a triple point exists at 230 °C and 3.6 kbar. Below this point crystals exist in the orthorhombic structure while above it crystals exist in the hexagonal structure.[12] High-pressure WAXD experiments have been conducted to isolate the hexagonal phase.[12−15] The hexagonal phase of PE has a characteristic *d*-spacing of 4.3 Å for the (100) reflection[14] while the orthorhombic phase has two characteristic *d*-spacings of 4.1 Å for the (110) reflection and 3.7 Å for the (200) reflection.[15] The conformation of the hexagonal phase has been studied by Raman spectroscopy[16−18] as well as by nuclear magnetic resonance.[19] The hexagonal phase, also referred to as the rotator or condis phase, consists of parallel packing of conformationally disordered chains. Within this packing, trans−gauche rotational isomers are randomly distributed with all-trans sequences of five or fewer CH_2 units in length.[16] This distribution of gauche segments allows for high degrees of mobility through rotation along the chain axis.[19]

While little analysis of ethylene−propylene copolymers can be found, the crystal structures of ultrahigh molecular weight polyethylene (UHMWPE) and ethylene−1-octene copolymers have been examined. It has recently been observed that ultrahigh molecular weight polyethylene can crystallize through a hexagonal mesophase into the orthorhombic phase below the reported triple point.[12] Occurrence of the hexagonal phase has also recently been reported in ethylene−1-octene copolymers containing 7.3 mol % 1-octene.[20] Wide- and small-angle X-ray scattering studies reveal the coexist-

---

* To whom correspondence should be addressed.

10.1021/ma001972u CCC: $20.00

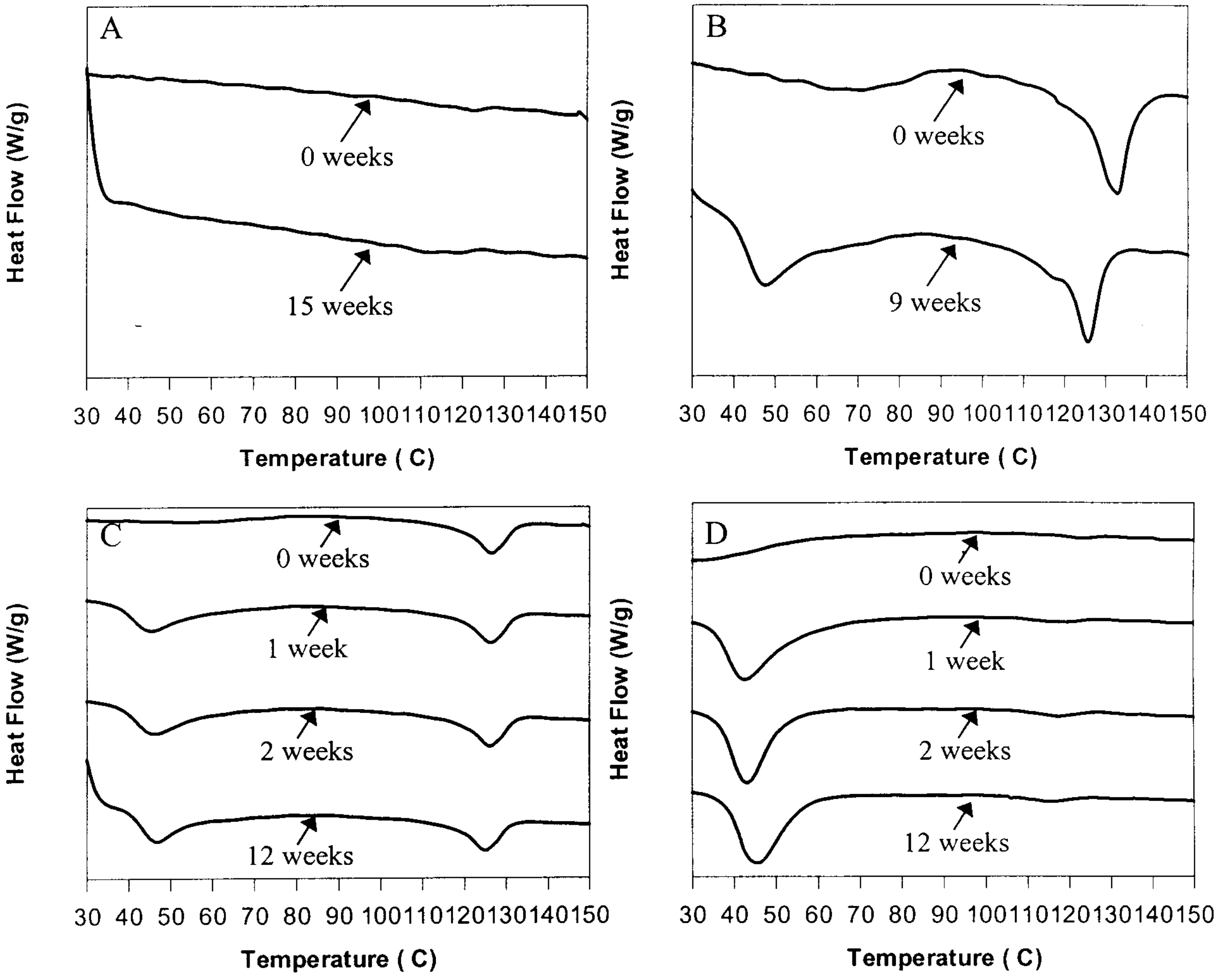

Figure 1. DSC thermograms of (a) sample A, (b) sample B, (c) sample C, and (d) sample D as a function of sample age.

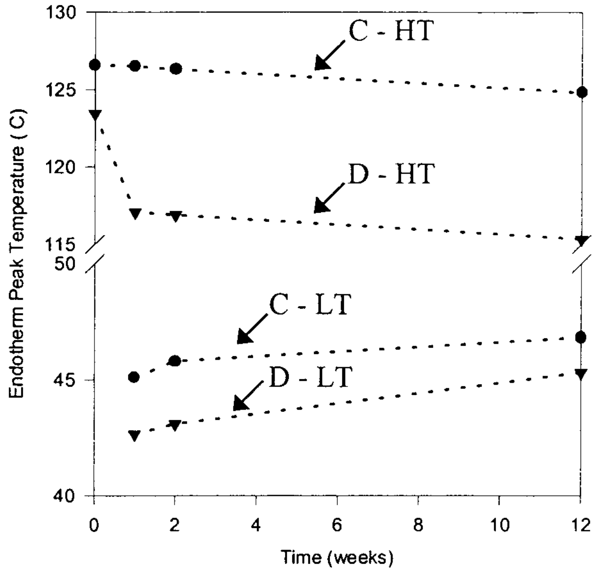

Figure 2. Demonstrates the shifts in the HT and LT endotherm positions as a function of time.

ence of orthorhombic and hexagonal crystal structures during drawing. The amount of hexagonal crystals increases upon drawing, and crystalline orientation is achieved. It is suggested that side chains excluded from the orthorhombic phase are accommodated by the hexagonal phase.[20]

It is well established that ethylene−α-olefin copolymers exhibit an "annealing" response when isothermally crystallized at ambient temperatures. It is accepted in industry that branched ethylene−propylene copolymers age at room temperature to achieve a maximum crystallinity; this is conventionally thought to occur over a 2 week period. For the context of this study the term "aging" will be used to merely describe the length of time between solidification and experimentation. Time zero is immediately after solidification, and the sample's age increases from this point until the maximum crystallinity is achieved. Little previous work has focused on correlating the evolution of crystal structure in ethylene−α-olefin copolymers with their changing mechanical properties.

While few results have been reported on the aging of ethylene-propylene copolymers, ethylene-1-octene random copolymers have recently been investigated.[10] A quenched sample exhibits a broad HT melting endotherm due to primary crystallization. Upon isothermal crystallization at room temperature for various times, heating thermograms reveal the emergence of a LT endotherm even for times as short as 1 min. As the crystallization time increases, the LT endotherm shifts to higher temperatures, and its heat of fusion increases. While the LT endotherm evolves, no change is observed in the position of the HT endotherm.[10]

The objective of this study is to examine crystal structure evolution in ethylene−propylene copolymers as a function of the aging process under ambient conditions. Additional studies are conducted to correlate

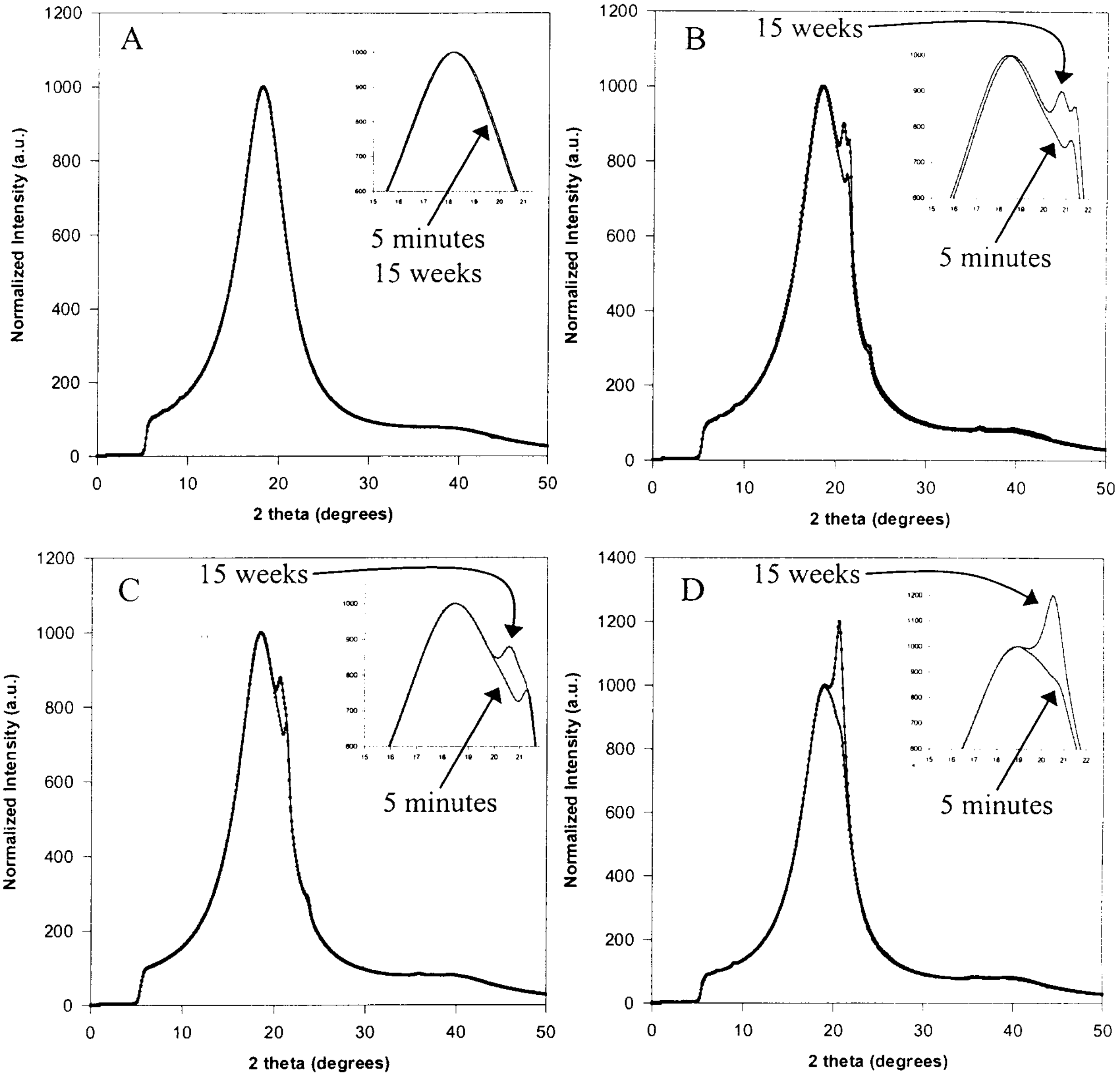

Figure 3. WAXD patterns for (a) sample A, (b) sample B, (c) sample C, and (d) sample D as a function of sample age.

changes in crystallinity and crystal structure with mechanical behavior and sample age. Four model compositions are examined where composition and comonomer distribution are systematically varied.

Experimental Section

Four ethylene−propylene random copolymer compositions are examined. The samples were produced by the ExxonMobil Chemical Co. using a Ziegler−Natta catalyst. The compositions are listed in Table 1 where ethylene content is given in mole percent together with molecular weights, polydispersity indices, and numbers of short chain branches per 1000 carbon atoms. Samples A and D are reported to have a more homogeneous or random comonomer distribution while samples B and C have a more heterogeneous or "blocky" structure. This difference in comonomer distribution is evident in their melting behavior and is discussed later.

Thermal analysis was performed using a Thermal Analysis 2910 differential scanning calorimeter (DSC). Indium was used as the calibration standard. Sample sizes between 5 and 8 mg were sealed in aluminum hermetic pans, and a nitrogen flow rate of 50 mL/min was maintained. All heating and cooling rates were 10 °C/min. DSC thermograms obtained immediately after solidification correspond to a second heating scan where samples were heated to 200 °C and equilibrated, cooled to 0 °C and equilibrated, and reheated to 200 °C. All other DSC thermograms obtained as a function of sample age correspond to first heating scans in order to preserve the crystallinity formed at room temperature.

Wide-angle X-ray diffraction (WAXD) measurements were performed on a Rigaku RU-H3R rotating anode X-ray diffractometer equipped with an Osmic multilayer focusing optic and an evacuated Statton-type scattering camera. The incident beam wavelength was 1.54 Å, corresponding to 8 keV Cu Kα radiation. Scattering patterns were acquired with 10 cm × 15 cm Fuji ST-VA image plates in conjunction with a Fuji BAS-2500 image plate scanner. Intensity profiles were obtained from radial averages of the scattering pattern intensities. Samples for WAXD were compression-molded into films approximately 0.6 mm thick at 190 °C for 10 min and then water-cooled.

Tensile tests were conducted on an Instron 1123. Monotonic tensile tests were conducted at a strain rate of 0.01 s^{-1}. All reported strains were calculated from crosshead displacement. Samples were compression molded into 3 mm thick plaques at 190 °C and a pressure of 3.5 MPa for approximately 20 min and water-cooled in the melt press. Tensile specimens were cut to an ASTM D638 type V geometry.

Table 2. LT and HT ΔHm and Estimated % Crystallinity

	after solidification			maximum		
sample	LT[a]	HT[a]	%[b]	LT[a]	HT[a]	%[b]
A	0	0	0	0	0	0
B	0	5.35	1.84	8.52	7.64	5.57
C	0	5.85	2.01	8.19	5.17	4.60
D	0	0.27	0.09	17.9	1.07	6.54

[a] Heat of fusion (J/g) from low and high temperature endotherms. [b] % crystallinity is based on the total heat of fusion (HT + LT) divided by the theoretical heat of fusion for PE crystals (290 J/g).

Results and Discussion

DSC. Melting behavior for the four compositions as a function of sample age is shown in Figure 1. To accurately compare the DSC scans as a function of sample age, all scans shown in Figure 1 were taken with the same set of samples (i.e., all samples were treated identically and left at room temperature for the time indicated). Figure 1a shows that sample A is an amorphous reference. Samples B and C shown in Figure 1b,c have a heterogeneous comonomer distribution and exhibit two melting endotherms. A HT endotherm is initially present in both of these samples while a LT endotherm develops over time. Sample D shown in Figure 1d has a more homogeneous comonomer distribution, and as such a negligible HT endotherm is observed while a substantial LT endotherm develops over time.

All of the compositions (except the amorphous reference) exhibit both a LT and HT endotherm that increase in size and shift in temperature. The upper endotherm shifts to lower temperatures as time progresses, and its area is only slightly increased; whereas, the lower endotherm shifts to higher temperatures, and its heat of fusion is drastically increased. The endotherm shifts are illustrated in Figure 2, which is a plot of the HT and LT endotherm peak temperatures for samples C and D as a function of time. It is apparent that for both samples the HT endotherm shifts to lower temperatures over time while the LT endotherm shifts to higher temperatures over time. It is also observed that the decrease in peak temperature for sample C occurs at a more uniform rate; whereas, that for sample D decreases rapidly during the first week, at which point the rate of decrease slows. The shift in the HT endotherm has not been reported prior to this study. Its exact origin has not yet been determined. However, since the heat of fusion of the HT endotherm increases with time and slight peak broadening is observed, smaller crystals could be forming, thus shifting the average peak position to lower temperatures. The development of a lower endotherm and its shift to higher temperatures with annealing time have been observed previously for ethylene−1-octene copolymers.[10]

Two crystalline regimes exist. Both endotherms are relatively broad, indicating a wide range of crystal sizes present. To compare the crystallinity between compositions, Table 2 shows the HT and LT endotherm heats of fusion (J/g) immediately after solidification and after the samples have reached maturity. The total heat of fusion is the sum of the HT and LT heats of fusion. The crystallinity of these samples should be compared in terms of their total heats of fusion since the theoretical value for these crystals is unknown. However, a rough estimate of crystallinity is determined and listed in Table 2 by utilizing the heat of fusion of a perfect orthorhombic crystal (290 J/g). Crystallinity increases in the order of sample A ≪ C < B < D.

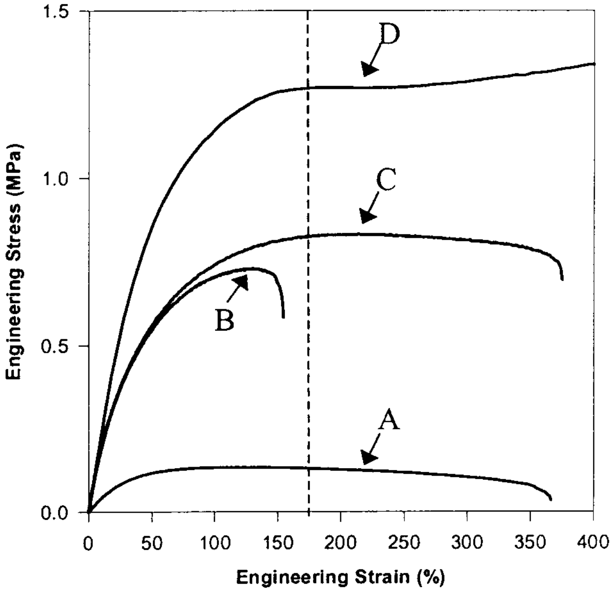

Figure 4. Engineering stress−strain curves for all four compositions illustrating "yieldlike" behavior and differences in ductility.

WAXD. WAXD measurements for the four compositions are shown in Figure 3 as a function of time. The inset in each of the plots in Figure 3 is a 2θ expansion of the peak between 15° and 22° in order to show changes that occur in the crystal structure over time. The WAXD results for sample A, the amorphous reference, are shown in Figure 3a. A very broad peak is observed at 2θ of 18.2°. This type of amorphous halo was also observed in another WAXD study on ethylene−α-olefin copolymers at 18.5°.[9] For the purposes of this study this peak is assigned as the amorphous halo for all compositions. As expected, no change is observed in the WAXD pattern for the amorphous sample as a function of time. Figure 3b shows the WAXD pattern for sample B as a function of time. Five minutes after solidification a small peak at 21.20° and a shoulder at 23.52° are observed. These two peaks correspond to the (110) and (200) reflections of orthorhombic polyethylene. After the sample has been aging at room temperature for 15 weeks, the WAXD pattern reveals the emergence of a peak at 20.56°. Using Bragg's law, this reflection corresponds to a *d*-spacing of 4.3 Å, which is the characteristic *d*-spacing of the (100) reflection for hexagonal polyethylene.[14] This hexagonal reflection is present in conjunction with the remaining orthorhombic (110) and (200) reflections. Figure 3c shows a similar evolution in crystal structure for sample C; except in this case only a shoulder corresponding to the (110) orthorhombic remains. The majority of the crystals present in sample C exist in the hexagonal phase. This is interesting considering that samples B and C are almost identical in composition. Figure 3d shows the WAXD patterns for sample D. Five minutes after solidification only a slight shoulder on the amorphous halo is observed, indicating very little crystallinity, which is consistent with DSC results. However, after 15 weeks a sharp peak has developed at 20.67° corresponding to the hexagonal (100) reflection.

It should be pointed out that the appearance of the hexagonal phase in these materials is occurring much

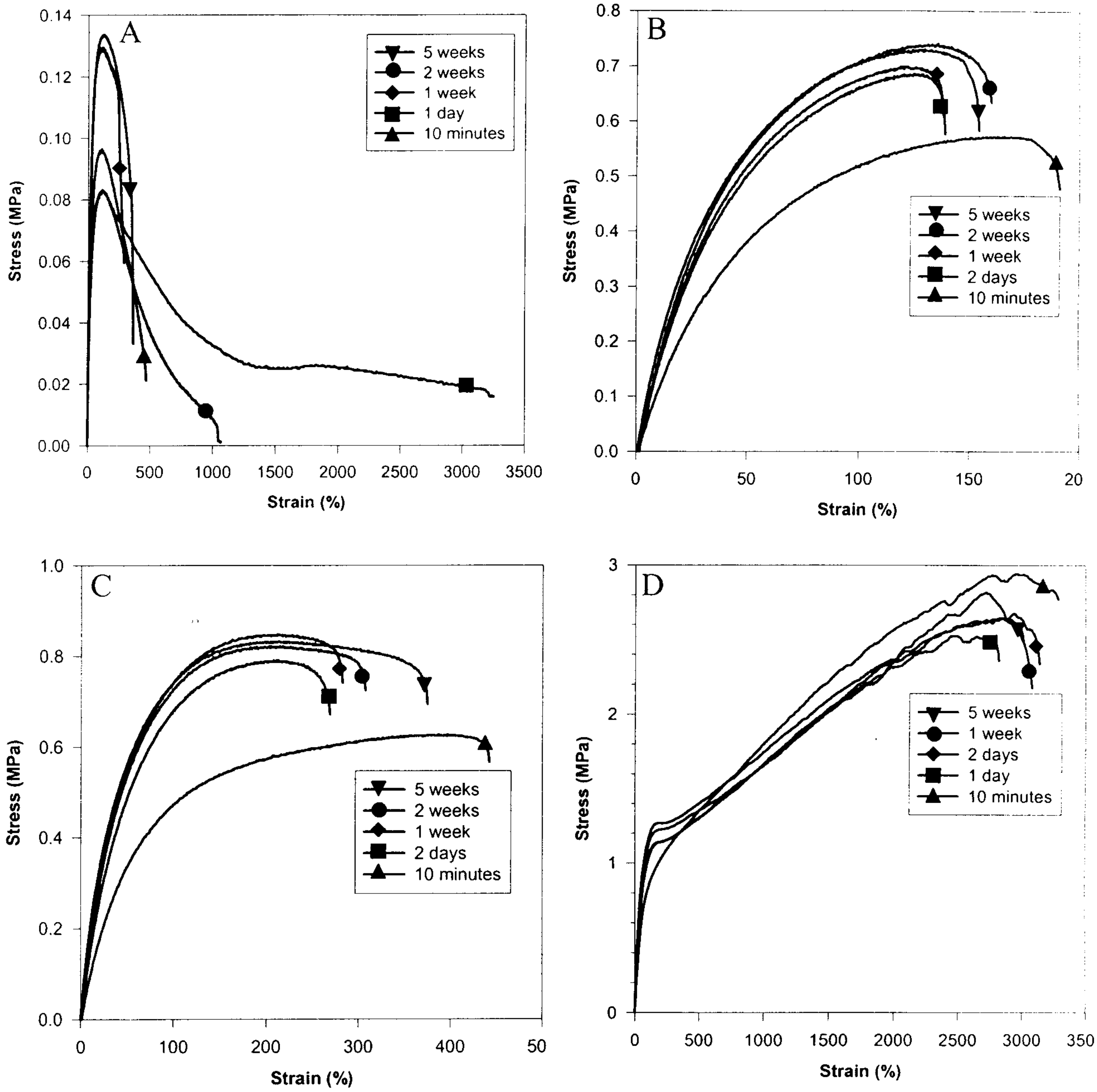

Figure 5. Engineering stress–strain curves for (a) sample A, (b) sample B, (c) sample C, and (d) sample D as a function of sample age.

below the triple point on the traditional PE phase diagram. The occurrence of the hexagonal phase below the triple point has also recently been observed in UHMWPE[11] and ethylene–1-octene copolymers.[20] This is the first observation of the coexistence of hexagonal and orthorhombic crystals in ethylene–propylene copolymers. Also, the crystal reflections present only correspond to the hexagonal and orthorhombic polyethylene structures; no polypropylene crystal structure is present. It should also be noted that the amorphous halo shifts to slightly larger 2θ values with additional incorporation of ethylene.

Mechanical Testing and Compositional Comparison. These materials are being considered as a new class of thermoplastic elastomers. In fact, their mechanical behavior is in between that of a true elastomer and a thermoplastic. They exhibit homogeneous deformation (no neck formation) like most elastomers but show “yieldlike” behavior similar to thermoplastics. Figure 4 presents an overlay of the engineering stress vs engineering strain curves for the four samples. The figure shows their yield responses in relation to composition. It should be pointed out that the full stress–strain curve is not shown for sample D which continues to strain harden. To describe this “yieldlike” behavior, the yield point is defined as the point on the stress–strain curve with zero slope. All of the compositions achieve a zero-slope condition that is approximately at a strain of 175%. Samples A and C have very similar molecular weights and as such demonstrate the same elongation at failure while sample B has a lower molecular weight and fails much earlier. The main difference between these materials is their ductility. While samples A, B, and C fail shortly after their respective yield points, sample D does not but continues to draw and strain harden to very high strains. Other studies not included here have interrogated the mechanical reversibility of these materials. They all exhibit substantial hysteresis loops when subjected to cyclic loading below their respective yield points, indicating the presence of dissipative mechanisms. Their reversibility is less than that of traditional cross-linked elastomers but greater than a typical thermoplastic (e.g., polypropylene).

Figure 5 shows engineering stress–strain curves for the four compositions, each as a function of time. The stress–strain curves for the amorphous reference, sample A, are shown in Figure 5a. Over a 5 week period the modulus ranges from 0.33 to 0.65 MPa with an average value of 0.47 ± 0.12 MPa. This composition resembles a viscous fluid, and as such the compression molded plaque thinned in some regions and not in others which accounts for the unexplainable trend in elongation at failure over the 5 week period. The stress–strain curves for samples B and C are shown in parts b and c of Figure 5, respectively. These two compositions behave similarly in the sense that 10 min after solidification they are relatively ductile and their moduli are low. As time progresses their moduli increase, and they become more brittle which can be explained by increased reinforcement due to evolving crystals. The modulus of sample B is consistently higher than that of sample C at all ages, which is also consistent with slightly higher amounts of crystallinity observed in DSC.

The stress–strain curves for sample D are shown in Figure 5d. This sample exhibits different crystallization kinetics where there is very little crystallinity immediately after solidification, and a large number of small crystals form over time, eventually giving sample D the highest crystallinity. Ten minutes after solidification the sample has a monotonically increasing stress–strain curve with no distinct yield point. The material is extremely ductile with a high elongation at failure. After 1 day the modulus has increased, and a distinct yield point has emerged. After 1 week, the yield stress has increased, but the yield strain remains constant. After 5 weeks the modulus and yield stress have again increased while the elongation at failure has essentially remained unchanged.

Various mechanical properties such as modulus, yield stress, yield strain, and rupture energy density are monitored as a function of sample age in order to determine correlations with crystal changes. Figure 6 plots modulus as a function of time for all four compositions. The modulus of the amorphous reference stays relatively constant over the 5 week period while the moduli of the other three samples increase rapidly within the first week. The rate at which the moduli increase after the first week is gradually reduced as the samples mature. Figure 7a plots the yield stress for samples B, C, and D as a function of time while Figure 7b plots the analogous yield strain as a function of time. For all three samples the yield stress increases within the first week and then remains relatively constant as the samples mature. The yield strain shows a different trend. For samples B and C the yield strain decreases rapidly within the first 2 days as the samples embrittle due to additional crystallinity. After 2 days, however, the yield strain remains constant while the yield stress continues to increase. Sample D behaves differently; its yield strain continues to increase within the first week exactly as its yield stress increases. After 1 week the yield strain for sample D again reaches a plateau. The rupture energy density of sample D is plotted as a function of time in Figure 8. The rupture energy density of sample D decreases exponentially as the sample ages in contrast to samples B and C where the rupture energy remains relatively constant within slight fluctuations (not shown on graph).

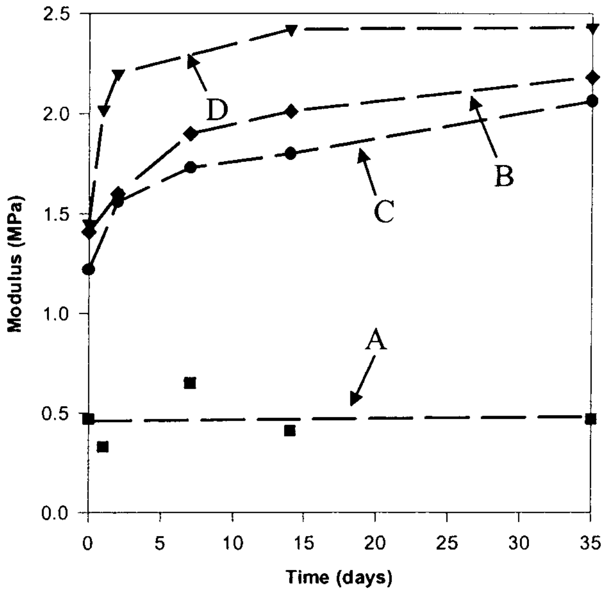

Figure 6. Modulus as a function of time for all four compositions.

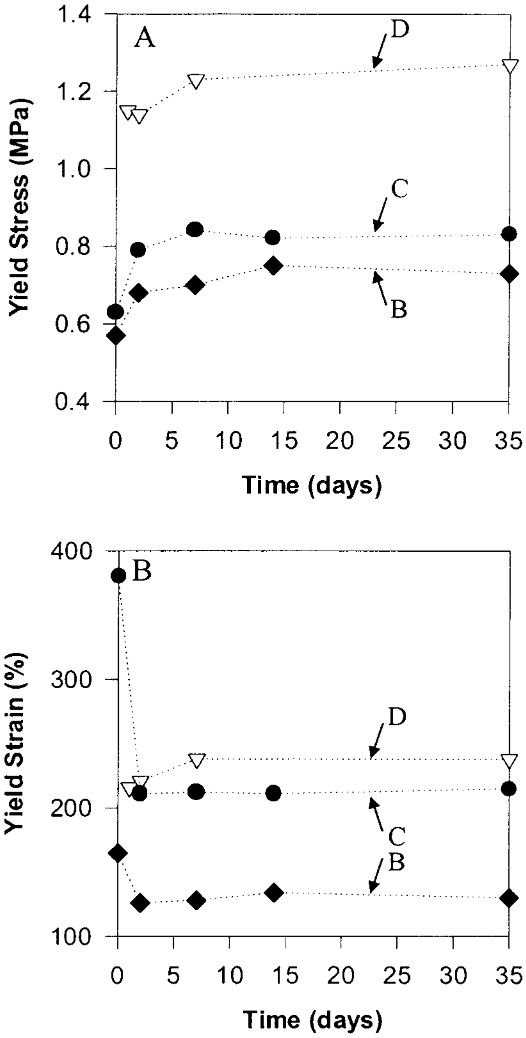

Figure 7. Demonstrates the shift in the (a) yield stress and (b) yield strain as a function of time.

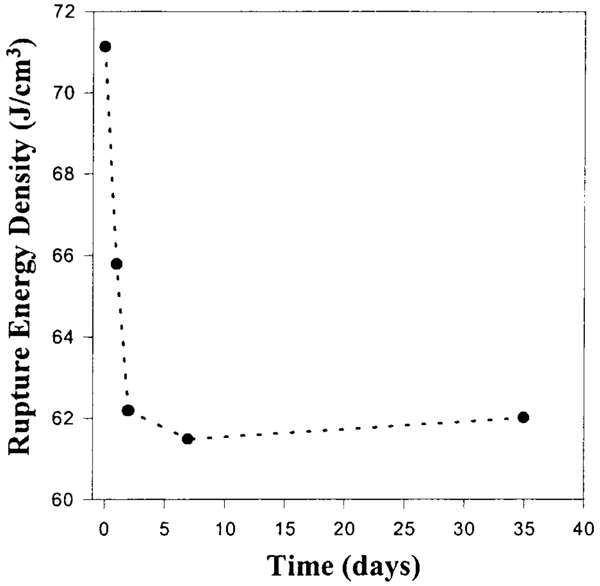

Figure 8. Rupture energy density as a function of sample age for sample D.

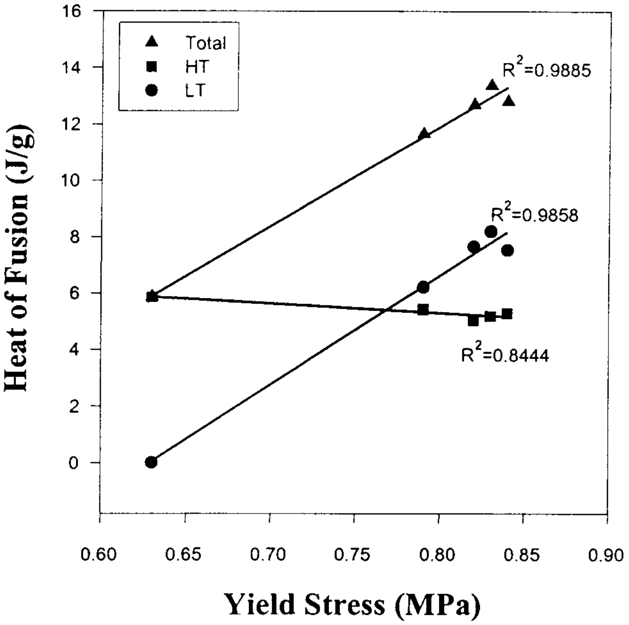

Figure 9. LT, HT, and total heats of fusion as a function of yield stress for sample C.

The mechanical properties are also examined in terms of the LT and HT endotherm heats of fusion as well as the total heat of fusion as a function of sample age. Figure 9 shows the LT, HT, and total heats of fusion as a function of yield stress for sample C. A linear regression is applied to the data. There is strong correlation between the LT endotherm and the yield stress; as the LT endotherm increases in size the yield stress also increases. There is relatively little correlation between the HT endotherm and the yield stress. Perfect superposition of the LT and HT data is observed in the total heat of fusion as a function of yield stress. Consequently, the data suggest that the changes in yield stress are primarily due to the changes in crystal morphology associated with the LT endotherm. The LT, HT, and total heats of fusion are plotted as a function of rupture energy density for sample D in Figure 10. Again, a strong correlation exists between the evolution of the LT endotherm and the decreasing rupture energy density. There is little dependence on the HT endotherm. Subsequently, the data again suggest that changes in rupture energy density are the result of changes in crystal morphology associated with the LT endotherm.

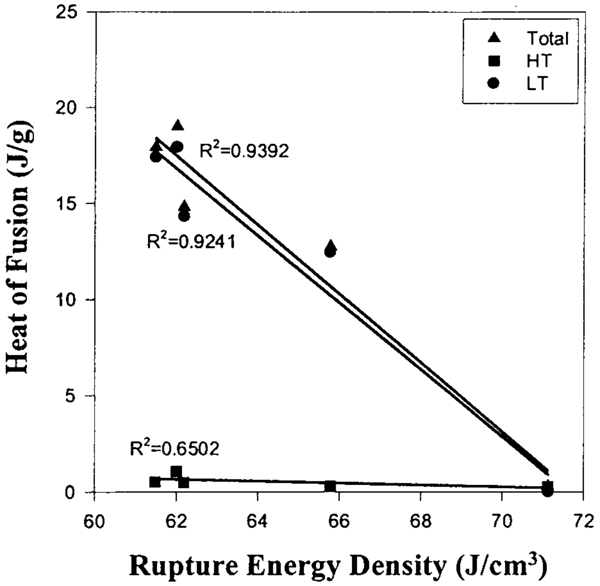

Figure 10. LT, HT, and total heats of fusion as a function of rupture energy density for sample D.

Conclusions

Crystal evolution and resulting mechanical behavior of four ethylene–propylene copolymers are examined. As the materials age at room temperature their crystal structure evolves from an orthorhombic structure to a hexagonal structure. Hexagonal and orthorhombic crystals coexist together in samples B and C while only the hexagonal phase is observed in sample D. The presence of the hexagonal and orthorhombic structures is directly related to the comonomer distribution. Samples B and C have a more blocky structure with longer ethylene segments that can form the orthorhombic structure while sample D has a more homogeneous comonomer distribution.

These materials exhibit mechanical behavior in between that of traditional elastomers and that of thermoplastics. The mechanical behavior evolution of these samples is characteristic of increasing crystallinity. The moduli increase as the samples age while the elongation at failure decreases. All samples show a “yieldlike” behavior. All of the materials yield at approximately the same strain. The main difference between the compositions is their postyield behavior. Samples A, B, and C fail shortly after yield while sample D continues to draw and strain harden. Increases in yield stress for samples B and C are the consequence of crystal evolution associated with the LT endotherm. These LT hexagonal crystals are also directly responsible for the decrease in rupture energy density as a function of time for sample D.

Acknowledgment. The authors acknowledge the ExxonMobil Chemical Co. for providing the materials for this study and for their permission to publish this paper. ExxonMobil as well as Advanced Elastomer Systems provided support for this study through the Center for UMASS/Industry Research on Polymers. The authors also acknowledge Dr. Andy Tsou and Dr. Michael Lyon for their guidance through out this study, Dr. Alan Waddon for his useful WAXD insight, and Dr. Helmut Strey for the use of his X-ray facility.

References and Notes

(1) Kim, M.-H.; Phillips, P. J. *J. Appl. Polym. Sci.* **1998**, *70*, 1893−1905.
(2) Wilfong, D.; Knight, G. W. *J. Polym. Sci., Polym. Phys.* **1990**, *28*, 861.
(3) Crist, B.; Claudio, E. S. *Macromolecules* **1999**, *32*, 8945−8951.
(4) Crist, B.; Williams, D. N. *J. Macromol. Sci., Phys.* **2000**, *B39*, 1−13.
(5) Bensason, S.; Minick, J.; Moet, A.; Chum, S.; Hiltner, A.; Baer, E. *J. Polym. Sci., Polym. Phys.* **1996**, *34*, 1301−1315.
(6) Wendling, J.; Suter, U. W. *Macromolecules* **1998**, *31*, 2516−2520.
(7) Kim, M.-H.; Phillips, P. J.; Lin, J. S. *J. Polym. Sci., Polym. Phys.* **2000**, *38*, 154−170.
(8) Alamo, R. G.; Chan, E. K. M.; Mandelkern, L. *Macromolecules* **1992**, *25*, 6381−6393.
(9) Vanden Eynde, S.; Mathot, V.; Koch, M. H. J.; Reynaers, H. *Polymer* **2000**, *41*, 3437−3453.
(10) Alizadeh, A.; Richardson, L.; Xu, J.; McCartney, S.; Marand, H. *Macromolecules* **1999**, *32*, 6221−6235.
(11) Swan, P. R. *J. Polym. Sci.* **1962**, *56*, 409−416.
(12) Rastogi, S.; Kurelec, L.; Lemstra, P. J. *Macromolecules* **1998**, *31*, 5022−5031.
(13) Galeski, A.; Bartczak, Z.; Argon, A. S.; Cohen, R. E. *Macromolecules* **1992**, *25*, 5705−5718.
(14) Bartczak, Z.; Galeski, A.; Argon, A. S.; Cohen, R. E. *Polymer* **1996**, *37*, 2113−2123.
(15) Turley, J. W. X-ray *Diffraction Patterns of Polymers*; Chemical Physics Research Laboratory: Michigan, 1965.
(16) Tashiro, K.; Sasaki, S.; Kobayashi, M. *Macromolecules* **1996**, *29*, 7460−7469.
(17) Kurelec, L.; Rastogi, S.; Meier, R. J.; Lemstra, P. J. *Macromolecules* **2000**, *33*, 5593−5601.
(18) Barnes, J. D.; Fanconi, B. M. *J. Chem. Phys.* **1972**, *56*, 5190−5192.
(19) Kuwabara, K.; Horii, F. *Macromolecules* **1999**, *32*, 5600−5605.
(20) Androsch, R.; Blackwell, J.; Chvalun, S. N.; Wunderlich, B. *Macromolecules* **1999**, *32*, 3735−3740.

MA001972U